Defect and Diffusion Forum Vol. 322 (2012) pp 151-162
Online available since 2012/Mar/15 at www.scientific.net

doi:10.4028/www.scientific.net/DDF.322.151

Influence of Deformation on Precipitation Kinetics in Mg-Tb Alloy

Oksana Melikhova[1, a], Jakub Čížek[1,b], Petr Hruška[1,c], Marián Vlček[1,d], Ivan Procházka[1,e], Martin Vlach[1,f], Ivana Stulíková[1,g], Bohumil Smola[1,h], Naďa Žaludová[1i], Rinat K. Islamgaliev[2,j]

[1]Faculty of Mathematics and Physics, Charles University, V Holešovičkách 2, CZ-180 00 Praha 8, Czech Republic

[2]Institute of Physics of Advanced Materials, Ufa State Aviation Technical University, Ufa 450 000, Russia

[a]oksivmel@yahoo.com, [b]jakub.cizek@mff.cuni.cz, [c]peta.hruska@gmail.com, [d]vlko.majo@centrum.sk,[e]ivan.prochazka@mff.cuni.cz, [f]martin.vlach@mff.cuni.cz, [g]ivana.stulikova@mff.cuni.cz, [h]bohumil.smola@mff.cuni.cz, [i]nadik.z@centrum.cz, [j]saturn@mail.rb.ru

Keywords: Mg alloys, precipitation hardening, positron annihilation, high pressure torsion.

Abstract. Precipitation effects in age-hardenable Mg-13wt.%Tb alloy were investigated in this work. The solution treated alloy was subjected to isochronal annealing and decomposition of the supersaturated solid solution was investigated by positron annihilation spectroscopy combined with transmission electron microscopy, electrical resistometry, differential scanning calorimetry and microhardness measurements. Peak hardening was observed at 200°C due to precipitation of finely dispersed particles of β'' phase with the $D0_{19}$ structure. Vacancy-like defects associated with β'' phase particles were detected by positron annihilation. At higher temperatures precipitation of β' and subsequently β phase takes place. Formation of these phases lead to some additional hardening and introduces open volume defects at precipitate/matrix interfaces. To elucidate the effect of plastic deformation on the precipitation sequence we studied also a Mg-13wt.%Tb alloy with ultra fine grained structure prepared by high pressure torsion. In the ultra fine grained alloy precipitation of the β'' phase occurs at lower temperature compared to the coarse grained material and the peak hardening is shifted to a lower temperature as well. This effect can be explained by enhanced diffusivity of Mg and Tb atoms due to a dense network of grain boundaries and high density of dislocations introduced by severe plastic deformation. Moreover, dislocations and grain boundaries serve also as nucleation sites for precipitates. Hence, precipitation effects are accelerated in the alloy subjected to severe plastic deformation.

Introduction

Mg-Tb is a promising light hardenable alloy with a high creep resistance at elevated temperatures. The maximum solubility of Tb in Mg is 24 wt.% at the eutectic temperature of 559°C, i.e. relatively large, but it rapidly decreases at lower temperatures, e.g. at 200°C it becomes only 9 wt.% [1]. By rapid quenching from elevated temperatures a supersaturated solid solution of Tb in Mg can be obtained. With increasing temperature the supersaturated solid solution α' decomposes obeying the following sequence [2]:

$$\alpha' \text{ (hcp)} \rightarrow \beta'' \text{ } (D0_{19}) \rightarrow \beta' \text{ (c-bco)} \rightarrow \beta \text{ (bcc, } Mg_{24}Tb_5). \quad (1)$$

The β'' transient phase with a hexagonal $D0_{19}$ structure is fully coherent with the hexagonal closed packed (hcp) Mg matrix and its lattice parameters are related to those of the Mg matrix as $a = 2a_{Mg}$, $c = c_{Mg}$. The β' transient phase exhibits c-base centered orthorhombic (c-bco) structure with lattice parameters $a = 2a_{Mg}$, $b \approx 8d(1\text{-}1\ 0\ 0)_{Mg}$, $c = c_{Mg}$. Particles of the β' phase are semicoherent with Mg matrix since in the (01-10) plane coherency is retained, but perpendicularly to this plane the coherency is lost. The stable β phase exhibits body centered cubic (bcc) structure and is incoherent with Mg matrix. The lattice mismatch between particles of semicoherent or incoherent phase and Mg matrix is compensated by open-volume misfit defects.

Formation of finely dispersed second phase particles may cause a significant hardening and improved strength of Mg alloys. Using rare earth alloying elements Mg alloys with favorable strength and thermal stability have been developed [3]. However, a remaining disadvantage of these alloys is a poor ductility insufficient for industrial applications. Grain refinement is a well-known method to improve the ductility of metals. Severe plastic deformation (SPD) applied in an appropriate way enables the achievement of an extreme grain refinement and is capable of producing bulk materials with ultra fine grained (UFG) structure, see [4] for a review. A number of techniques based on SPD have been developed so far, however the strongest grain refinement was achieved by high pressure torsion (HPT) [5]. Extremely small grain size (~100 nm) leads to a significant volume fraction of grain boundaries which represent obstacles for movement of dislocations and cause a significant hardening additional to the age hardening effect caused by precipitates. As a consequence, the UFG metals are often characterized by a favorable combination of a very high strength and a reasonable ductility [4].

Precipitation effects are influenced by concentration of nucleation sites and by the diffusivity of solutes. Dislocations enhance both these parameters. Therefore, a high dislocation density introduced by SPD may influence the precipitation processes. To elucidate this effect in this work we performed a detailed investigation of precipitation effects in conventional coarse-grained Mg-Tb alloy and in UFG Mg-Tb alloy prepared by HPT.

Since defects play a very important role in the UFG materials we employed positron lifetime (LT) spectroscopy as a powerful tool for defect studies on the atomic scale. The LT spectroscopy is a well developed non-destructive technique with a high sensitivity to open volume defects (e.g. vacancies, dislocations etc.) and allows for identification of defects and determination of defect densities in the studied material [6]. In the present work, LT spectroscopy was combined with Vicker's microhardness (HV) testing, electrical resistometry, differential scanning calorimetry (DSC) and transmission electron microscopy (TEM).

Experimental

Samples. Binary Mg-13wt.%Tb (Mg13Tb) alloy was produced by squeeze casting under a protective gas atmosphere (Ar + 1%SF_6). The as-cast alloy was solution treated at 530°C for 6h in a vertical furnace with a protective Ar atmosphere. The solubility of Tb in Mg is 22 wt.% at 530°C and annealing for 8h was found to be sufficiently long to dissolve Tb completely in the Mg matrix [7]. The solution treatment was finished by quenching into water of room temperature. The content of Tb determined in the solution treated sample by chemical analysis was 13.3 wt.%.

Another solution treated Mg13Tb sample was deformed by HTP at room temperature using hydrostatic pressure of 6 GPa and performing 5 HPT revolutions.

Methods of characterization. Positron lifetime (LT) investigations were performed using a fast-fast LT spectrometer equipped with BaF_2 scintillators and Photonis XP2020/Q photomultipliers. The LT spectrometer exhibits excellent time resolution of 150 ps (FWHM ^{22}Na) and its detailed description is given in Ref. [8]. At least 10^7 annihilation events were accumulated in each LT spectrum using ≈ 1 MBq $^{22}Na_2CO_3$ positron source deposited on a 2 μm thick mylar foil. The TEM observations were carried out on a JEOL 2000 FX electron microscope operating at 200 kV. A Struers Duramin 300 hardness tester was employed for microhardness measurements by Vicker's technique using a load of 100 g applied for 10 s. Relative changes of electrical resistivity were

measured by the standard four-point method at 77 K with a dummy specimen in series. The influence of parasitic thermopowers was suppressed by the commutation of the measuring current. Relative electrical resistivity changes $\Delta\rho/\rho_0$ were obtained to an accuracy of 10^{-4}. DSC investigations were carried out on a Netsch DSC 200 F3 apparatus with Al_2O_3 crucibles. DSC curves were measured at various heating rates from 1 K/min to 20K/min in a nitrogen protective atmosphere.

Isochronal annealing. After characterization of the initial state (i.e. solution-treated or as-deformed sample) the samples was subjected to step-by-step isochronal annealing. For LT and HV measurements the isochronal annealing was performed in steps 20°C/20 min, while for electrical resistometry 30°C/30 min steps were used. Hence, in all cases the effective heating rate was 1 K/min. Annealing was performed in silicon oil bath up to 250°C and in an electrical furnace at higher temperatures. Each annealing step was finished by quenching into water. Subsequent LT, HV and TEM investigations were performed at room temperature. Electrical resistometry was performed in liquid nitrogen at temperature 77 K. DSC measurements were performed with heating rates 1, 2, 5, 10 and 20 K/min. From positions of the DSC peaks at various heating rates the activation energy of undergoing precipitation process was determined using the Kissinger's plot.

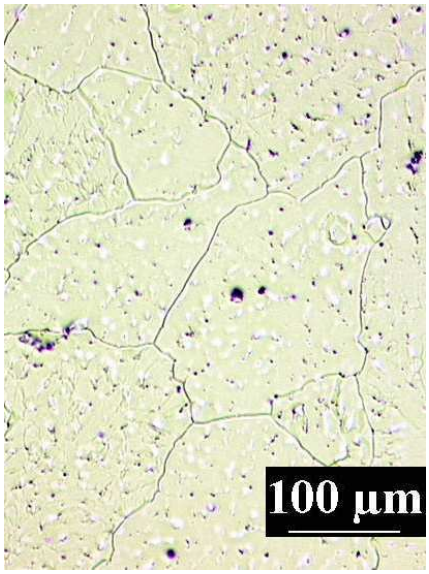

Figure 1 Light microscopy image of solution-treated Mg13Tb alloy.

Results

Solution treated alloy. Fig. 1 shows light microscopy image of solution treated alloy. The sample exhibits a coarse grain size around 100 μm. Hardness decreased after solution treatment from the value HV = 88 ± 3 measured in the as cast alloy down to HV = 75 ± 3. This is obviously due to recovery of dislocations created during casting and cutting and dissolution of precipitates existing in the as-cast alloy. A single component spectrum with positron lifetime of 222.0 ± 0.5 ps was measured on the solution treated alloy by LT spectroscopy. This lifetime is in a reasonable agreement with the bulk positron lifetime in well-annealed Mg [9] which testifies that the solution treated alloy exhibits a very low density of defects.

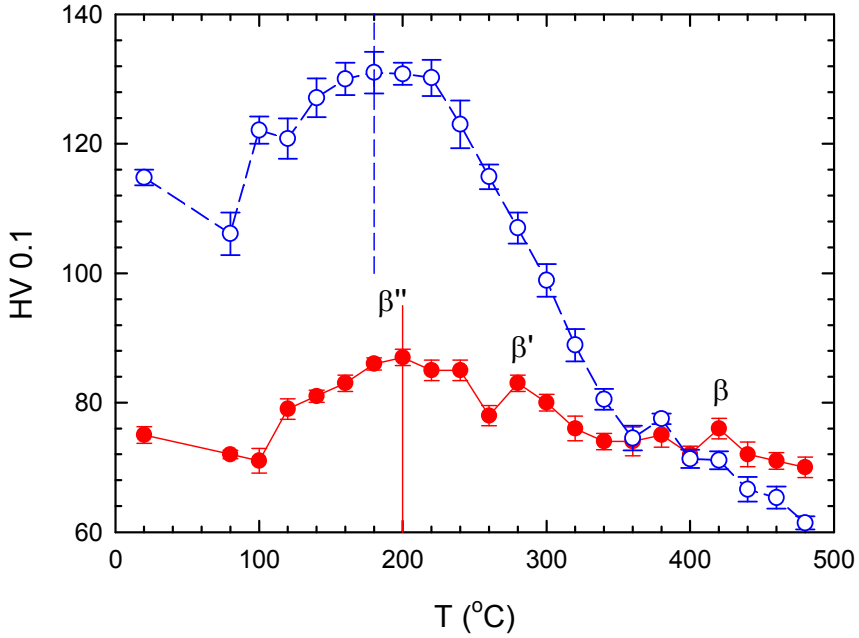

Figure 2 Temperature dependence of microhardness in solution treated alloy (full points) and HPT-deformed alloy (open points). Peak hardening temperature in solution treated and HPT-deformed alloy is indicated by the solid and dashed line respectively.

The temperature dependence of HV measured on the solution treated alloy subjected to isochronal annealing is plotted in Fig. 2, while Fig. 3(A) shows relative changes of electrical resistivity $\Delta\rho/\rho_0$. The negative derivative of the electrical resistivity curve with respect to temperature (so-called resistivity annealing spectrum) is plotted in Fig. 3(B). A significant rise of HV occurs after annealing above 100°C, see Fig. 2, and is accompanied by a strong decrease of electrical resistivity in the temperature range 80 - 180°C. This gives clear evidence that precipitation takes place in the sample. Indeed, TEM investigations performed on the sample annealed at 180°C revealed precipitation of the transient β'' phase with $D0_{19}$ structure. However, β'' phase particles are too fine to be resolved in the bright-field TEM image, see Fig. 4(A), and could be identified only from the electron diffraction pattern which is shown in Fig. 4(B). Very small size of β'' phase particles is demonstrated also by diffusion character of the diffraction spots in Fig. 4(B).

In the Mg13Tb alloy annealed above 100°C an additional component with lifetime $\tau_2 \approx 256$ ps appeared in the LT spectrum. This testifies that new defects were created in the sample and some positrons annihilated in trapped state at these defects. The temperature dependence of the relative intensity I_2 of positrons trapped at defects is plotted in Fig. 5. The lifetime $\tau_2 \approx 256$ ps represents a contribution of positrons trapped at vacancy-like defects associated with β'' phase particles [9]. Hence, although β'' phase is coherent with Mg matrix, in the early stages of precipitation the β'' phase particles contain vacancy-like defects. This is not surprising since the formation of β'' phase particles occurs by thermally activated diffusion of Tb atoms via the vacancy mechanism. Hence, in the early stages of precipitation the structure of the β'' phase particles is far from being perfect and contains vacancies. Similar effect was observed in the early stages of precipitation in Mg-Gd alloys [9]. The intensity of positrons trapped at vacancy-like defects achieves a maximum at 180°C. Annealing at higher temperatures leads to a development of the β'' phase precipitates with a well defined structure and vacancies are gradually annealed out which is reflected by a decrease in intensity of positrons trapped at defects.

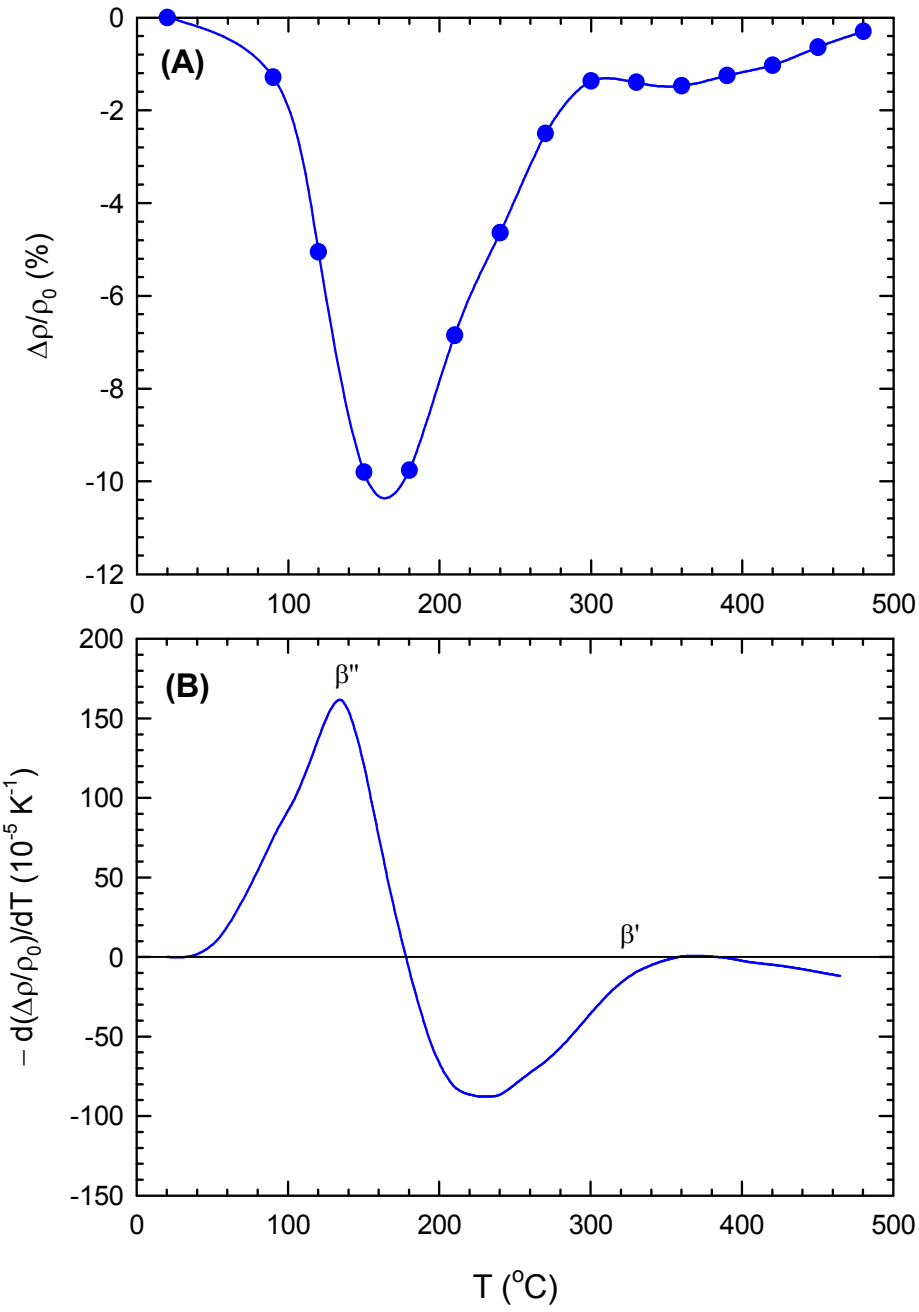

Figure 3 Results of electrical resistometry for solution-treated Mg13Tb alloy: (A) relative changes of electrical resistivity $\Delta\rho/\rho_0$ for the sample subjected to isochronal annealing, (B) annealing spectrum of electrical resistivity, i.e. the negative derivative of the relative changes of electrical resistivity with respect to temperature.

One can see in Fig. 2 that peak hardening is achieved at 200°C. Further annealing at higher temperatures leads to a decrease in HV due to growth and/or dissolution of the β'' phase particles. Dissolution of the β'' phase particles is testified also by an increase of electrical resistivity which is clearly seen in Fig. 3(A).

From comparison of HV and LT measurements one can notice that the intensity of trapped positrons becomes maximal at 180°C, i.e. at temperature about 20°C lower than the peak hardening temperature. This happens because the maximum hardening is achieved when finely dispersed coherent precipitates with well defined relationship with the Mg matrix are developed, while contribution of trapped positrons is largest for β'' phase particles with a defected structure formed

in the early stages of precipitation. The maximum rate of the resistivity decrease is achieved already at temperature of 140°C and corresponds to the peak position in the resistivity annealing spectrum plotted in Fig. 3(B). This happens because the resistivity is strongly influenced by the concentration of Tb atoms dissolved in Mg matrix, which drops in the early stages of precipitation due to clustering of Tb atoms.

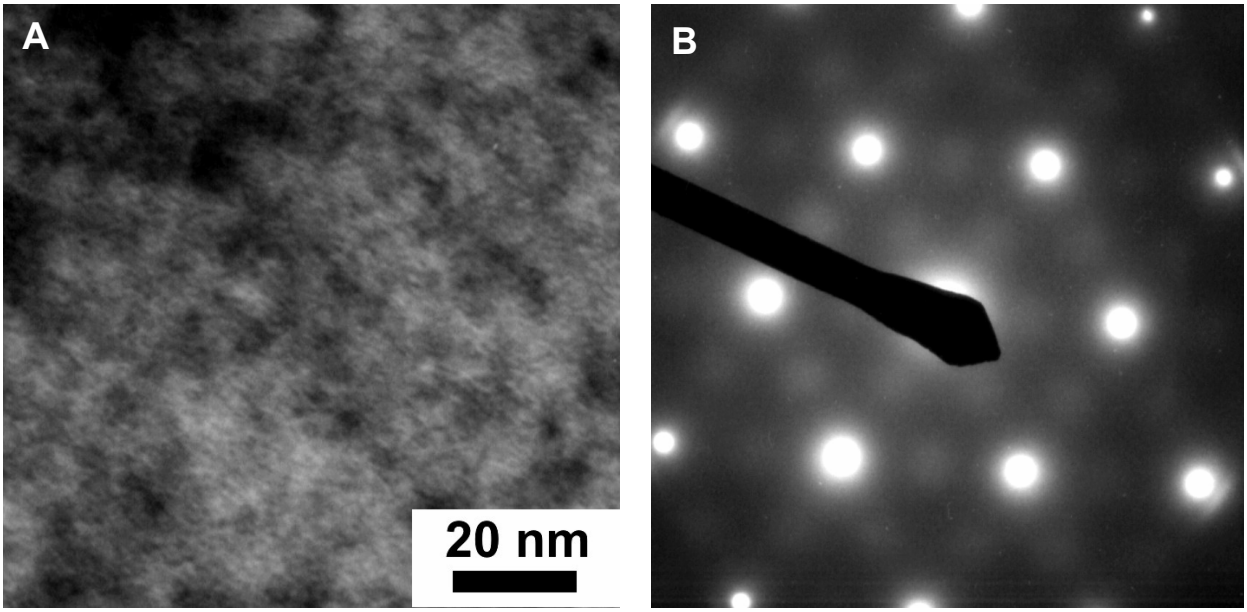

Figure 4 Microstructure of solution-treated Mg13Tb alloy annealed at 180°C: (A) a bright-field TEM image, (B) selected area electron diffraction pattern in [0001] orientation containing in addition to diffraction spots from Mg matrix also diffuse spots corresponding to fine β'' phase particles with $D0_{19}$ structure.

A single exothermic peak was observed on DSC annealing curves measured at various heating rates. For the heating rate dT/dt = 1 K/min (i.e. the same heating rate as that used in LT, HV and electrical resistivity measurements) the maximum of this peak was observed at temperature of 140°C which testifies that the process of β'' phase formation was detected by DSC. With increasing heating rate the temperature T_m corresponding to the maximum of the DCS peak was shifted to higher temperatures. DSC data were analyzed using the Kissinger method [10]. For a single precipitation process the peak temperature T_m obeys the equation:

$$\ln\left(\frac{dT}{dt}\frac{1}{T_m^2}\right) = -\frac{E}{RT_m} + C, \qquad (2)$$

where C is a constant, E is the activation energy of the precipitation process, and R the gas constant. Fig. 6 shows the Kissinger plot, i.e. $\ln[(dT/dt)(1/T_m)^2]$ plotted versus $1/T_m$, created using the data from the DSC curves measured at various heating rates. Obviously the points in the Kissinger plot fall on a straight line, which testifies that Eq. (2) holds, see Fig. 6. From the slope of the Kissinger plot one obtains the activation energy for the formation of the β'' phase precipitates E = (97 ± 4) kJ mol.$^{-1}$ This value is higher than the activation energy of ≈ 75 kJ mol^{-1} determined for Guinier-Preston zone formation in Mg-Nd alloy [11] but agrees well with the activation energy for precipitation of β'' phase plates with $D0_{19}$ structure in Mg–Nd–Gd–Zr alloy (111 ± 2) kJ mol^{-1} determined recently by SAXS [12]. This supports the picture that the exothermic peak observed in DSC annealing curves can be attributed to the formation of the β'' phase precipitates.

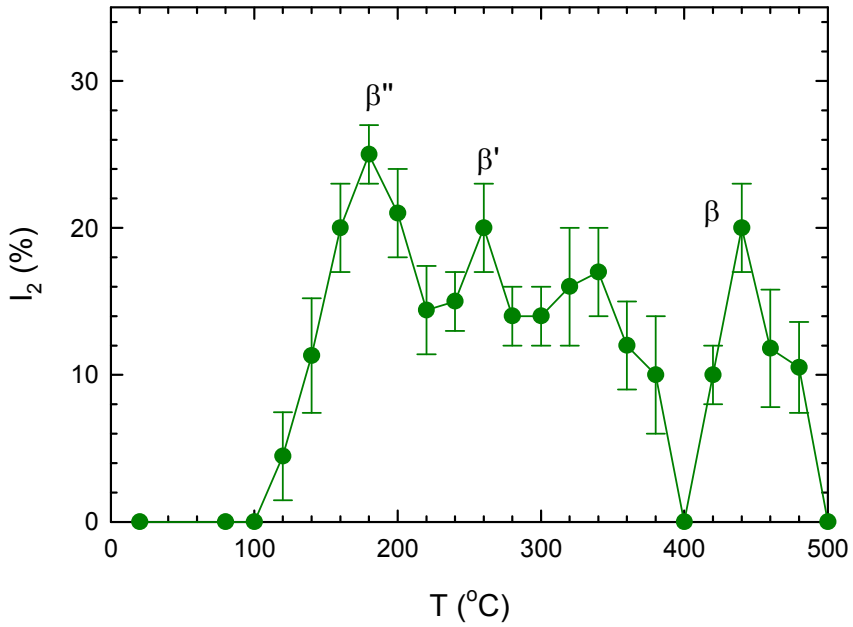

Figure 5 Results of LT measurements of solution-treated Mg13Tb alloy subjected to isochronal annealing: temperature dependence of intensity I_2 of positrons trapped at defects.

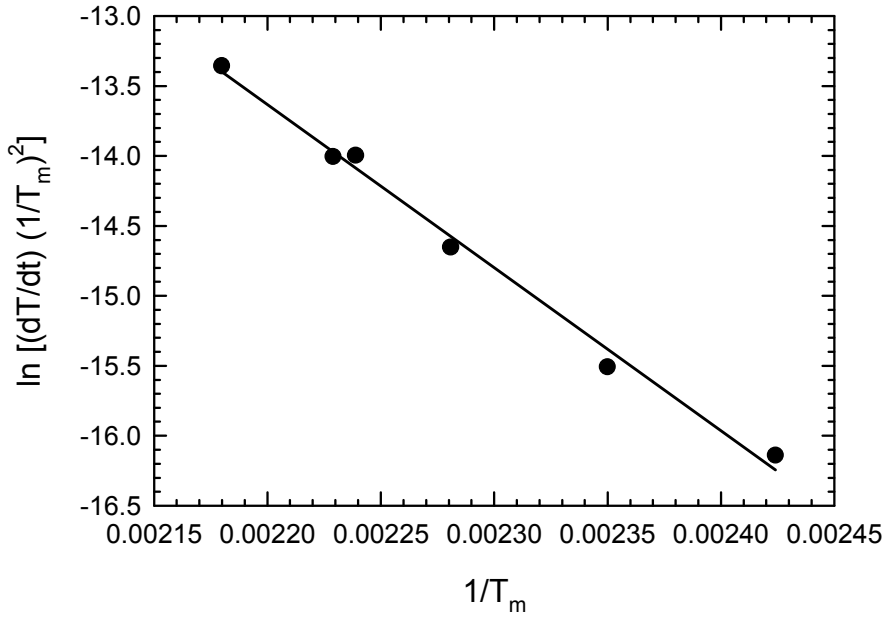

Figure 6 Kissinger plot constructed from positions T_m of peaks corresponding to formation of β'' phase in the DSC annealing curves measured with various heating rates dT/dt.

One can see in Fig. 2 that after a drop at 260°C HV increases again with temperature and exhibits a local maximum at 280°C caused by precipitation of the β' phase with c-bco structure. Since the β' phase precipitates are semi-coherent with the Mg matrix misfit defects are created at the interfaces which are not parallel with the (01-10) plane. Because of positron trapping at misfit-defects,

precipitation of the β' phase is accompanied by an increase in the intensity of positrons trapped at vacancy-like defects, see Fig. 5. Since the volume fraction of β' phase formed in Mg13Tb alloy is relatively low, there is only a slight response of electrical resistivity to formation of this phase (see Fig. 3). Because of the same reason it was impossible to detect the formation of the β' phase on DSC annealing curves.

Annealing above 280°C leads to growth and subsequently dissolution of the β' phase precipitates which is accompanied by decreasing HV and the intensity of positrons trapped in misfit defects. Complete dissolution of the β' phase occurs at 400°C where I_2 becomes zero.

At elevated temperatures above 400°C there is a very slight hardening peak caused by precipitation of the stable β phase. This is accompanied by a rise of the intensity I_2 because positrons are trapped at misfit defects created between incoherent β phase precipitates and Mg matrix. The formation of β phase could not be detected by electrical resistivity and DSC due to low volume fraction of precipitating particles. Finally at 500°C the solid solution of Tb in Mg is restored.

HPT-deformed alloy. In HPT processing, a disk-shaped sample with diameter of 10 mm located between two anvils is subjected to a compressive pressure of several GigaPascals (here 6 GPa) and simultaneously strained by a rotating anvil. The shear strain imposed on the disk during HPT processing increases with the radial distance r from the sample disk center (corresponding to the rotation axis). The homogeneity of HPT-deformed specimen across the sample disk was checked by HV measurement at various distances r from the centre. As shown in Fig. 7 no systematic variations of HV with r were observed. Hence, the structure of HPT-deformed sample can be considered as reasonably uniform across the whole sample disk.

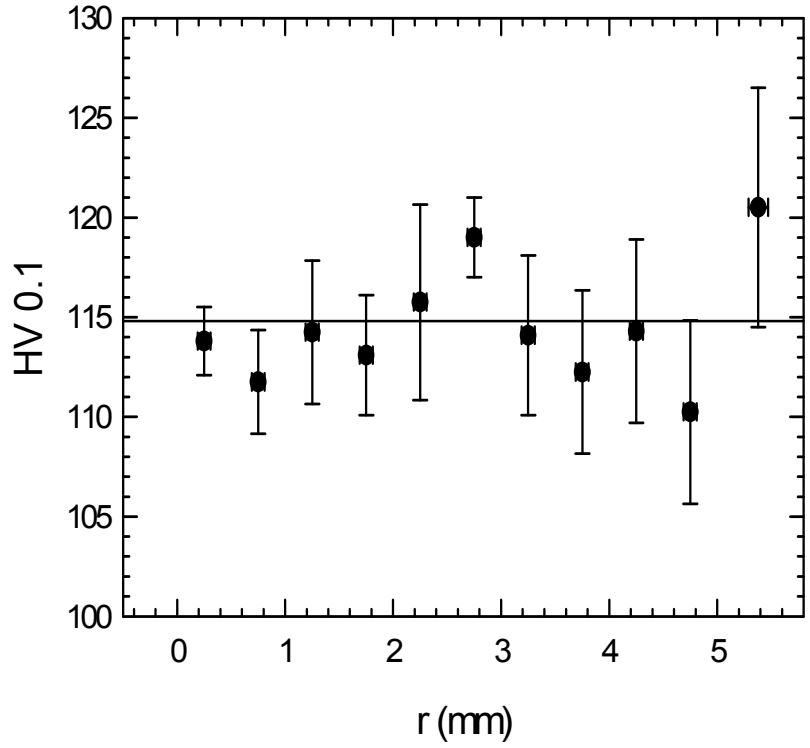

Figure 7 Dependence of microhardness HV on the radial distance r from the center of the HPT-deformed sample disk. Each point in the figure was calculated as an average of several measurements at various points on the sample with the same distance from the center.

A TEM micrograph of HPT-deformed Mg13Tb alloy is shown in Fig. 8. The sample exhibits UFG structure with a mean grain size ≈100 nm and a high density of dislocations introduced by severe plastic deformation. The electron diffraction pattern (inset in Fig. 8(A)) testifies high-angle miss-orientation of neighboring grains. No precipitates were observed in the as-deformed sample by TEM, i.e. it can be considered as a supersaturated solid solution of Tb in Mg. HPT-deformed sample exhibits hardness of 115 ± 1, which is about of 50% higher than in the solution-treated alloy. This substantial hardening is due to grain refinement and dislocations introduced by HPT deformation. The LT spectrum of HPT-deformed sample consists of a shorter component with lifetime $\tau_1 \approx 210$ ps representing a contribution of free positrons and a longer component with lifetime $\tau_2 \approx 256$ ps and relative intensity $I_2 \approx 50$ % which comes from positrons trapped at dislocations. Using the two state trapping model [6] and the specific trapping rate for dislocations in Mg $\nu = 1 \times 10^{-4}$ m^2s^{-1} [13] dislocation density of $(1.5 \pm 0.5) \times 10^{14}$ m^{-2} was estimated in the HPT-deformed sample.

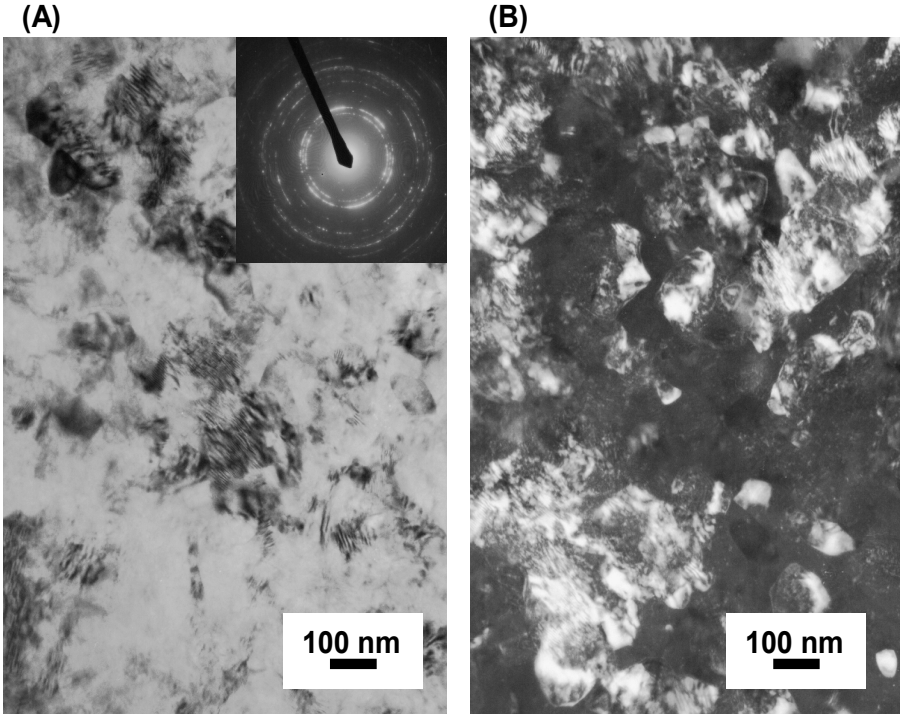

Figure 8 Microstructure of HPT-deformed Mg13Tb alloy: (A) bright field TEM image, (B) dark field image; electron diffraction pattern is shown in the inset.

The temperature dependence of microhardness in HPT-deformed Mg13Tb alloy subjected to isochronal annealing is plotted in Fig. 2 (open points). The hardening peak due to precipitation of finely dispersed coherent particles the β'' phase is clearly visible. Moreover, from inspection of Fig. 2 one can conclude that precipitation of the β'' phase starts already at 100°C, i.e. at about of 20°C lower temperature than in the coarse-grained alloy. Also the peak hardening in HPT-deformed sample is achieved at a lower temperature than in the coarse-grained alloy, see Fig. 2. This effect is obviously due to UFG structure and high dislocation density in HPT-deformed alloy. The significant volume fraction of grain boundaries and high dislocation density enhances the diffusivity of Mg and Tb atoms due to diffusion along grain boundaries or dislocation lines. Moreover, dislocations may serve as nucleation centers for precipitates. Due to these factors precipitation of the β'' phase is accelerated in HPT-deformed alloy. Moreover, the precipitation hardening caused

by the β'' phase in HPT-deformed sample is ΔHV = 25 ± 3, which is about 60% higher than in the solution treated alloy (ΔHV = 16 ± 2). This indicates that β'' phase particles in HPT-deformed sample are finer than in the coarse-grained alloy due to higher density of nucleation sites.

Above 220°C recrystallization takes place in the HPT-deformed sample leading to a significant softening since deformed UFG matrix with high dislocation density is gradually replaced by coarser dislocation-free recrystallized grains. The hardening peak caused by precipitation of the β' phase is hidden in HPT-deformed alloy due to softening by recrystallization occurring simultaneously, see Fig. 2. Recrystallization in HPT-deformed sample is finished at 360°C and hardness becomes comparable with that of coarse-grained alloy.

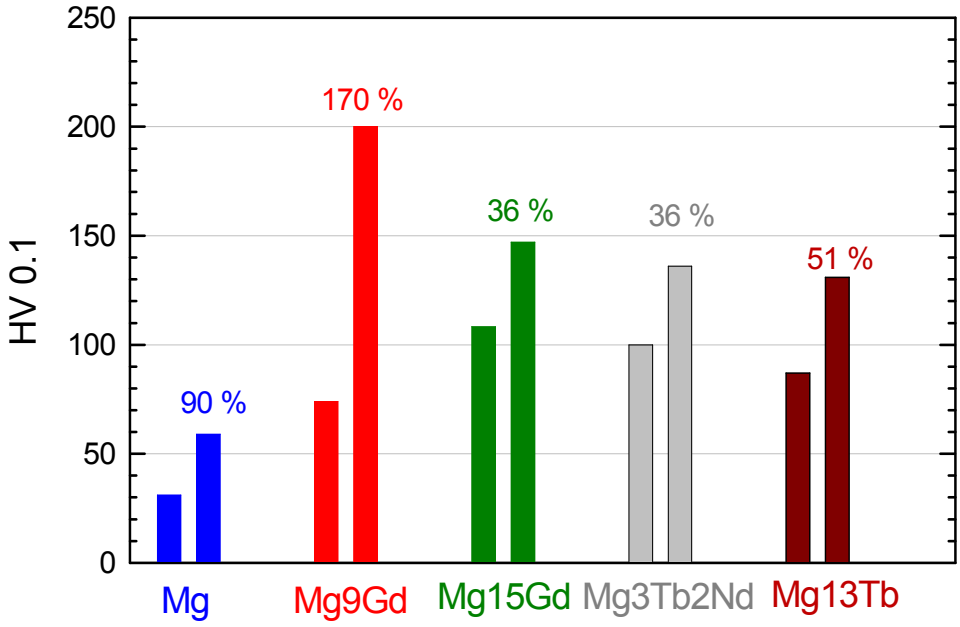

Figure 9 Comparison of peak hardness for conventional coarse grained samples (left vertical bars) and HPT-deformed samples (right vertical bars) for pure Mg and various Mg-alloys with rare earth alloying elements. The numbers in the figures show relative increase of peak hardness in HPT-deformed sample.

Discussion

Comparison of precipitation processes in Mg13Tb alloy in solution-treated state characterized by coarse grains and very low dislocation density and HPT-deformed sample which exhibits UFG structure and high density of dislocations revealed that precipitation is enhanced in the HPT-deformed alloy due to the higher diffusivity of Mg and Tb atoms and due to the high density of nucleation centers for the second phase particles. As a consequence, precipitation of metastable phases occurs at lower temperatures in HPT-deformed samples than in common coarse-grained alloys. This seems to be a general phenomenon which was observed also in other age-hardenable Mg alloys with rare earth alloying elements. For example, the peak hardening in HPT-deformed Mg-9wt.%Gd occurs at temperature which is about of 80°C lower than peak hardening temperature in a coarse-grained alloy [14]. Similarly peak hardening in HPT-deformed Mg-3wt.%Tb-2wt.%Nd alloy was found to be shifted to 100°C lower temperature compared to the corresponding coarse-grain alloy [15]. Detailed investigations of Mg-15wt.%Gd alloy subjected to various deformation [16] revealed that the shift of peak hardening to lower temperatures becomes more pronounced with increasing strain.

Moreover, the hardness of HPT-deformed Mg-alloys is significantly higher than the peak hardness of their coarse grained counterparts. This is demonstrated in Fig. 9 which shows a comparison of the peak hardness achieved in coarse grained alloy and HPT-deformed sample. Obviously Mg-alloys with UFG structure exhibits enhanced peak hardness. This is due to the combined effect of hardening due to very small grain size, high density of dislocations and in most cases also a finer size of second phase precipitates formed during age hardening. Interestingly, because of the UFG structure HPT-deformed Mg-alloys exhibit not only higher hardness but also enhanced ductility compared with the coarse grained alloys [17]. Obviously this is very important for improving of the workability of age-hardenable Mg-alloys which is still not satisfactory.

Summary

Precipitation effects in coarse-grained Mg13Tb alloy and HPT-deformed alloy with UFG structure were investigated. It was found that peak hardening in Mg13Tb alloys is caused by precipitation of finally dispersed β'' phase with $D0_{19}$ structure. Formation of β'' phase was detected also by electrical resistometry and differential scanning calorimetry. Positron lifetime spectroscopy revealed that in the early stages of precipitation β'' phase particles contain vacancy-like defects. Further precipitation of semi-coherent β' phase and incoherent β phase has a smaller hardening effect and introduces misfit defects at precipitate/matrix interfaces. In HPT-deformed alloy precipitation of β'' phase occurs at lower temperature due to enhanced diffusivity of Mg and Tb atoms and β'' phase particles are finer because of the higher density of nucleation sites.

Acknowledgement

This work was supported by the Czech Science Foundation (projects P108/10/0648, 106/09/0407 and P108/12/G043) and the Academy of Science of Czech Republic (project KAN300100801).

References

[1] L.L. Rokhlin, Magnesium Alloys Containing Rare Earth Metals, Taylor and Francis, London (2003).

[2] G.W. Lorimer, Proc.of the London Conference Mg Technology, London (1986), p. 47.

[3] B.L. Mordike: Mat. Sci. Eng. A Vol. 324 (2002), p. 103.

[4] R.Z. Valiev, R.K. Islamgaliev, I.V. Alexandrov: Prog. Mat. Sci. Vol. 45 (2000), p. 103.

[5] A.P. Zhilyaev, T.G. Langdon, Prog. Mater. Sci. Vol. 53 (2008) p. 893.

[6] P. Hautojärvi, C. Corbel, in: *Proc. International School of Physics "Enrico Fermi", Course CXXV*, edited by A. Dupasquier, A.P. Mills, IOS Press, Varena (1995), p. 491.

[7] I. Stulíková, B. Smola, N. Žaludová, M. Vlach, J. Pelcová, Kovov. Mater. Vol. 43 (2005), p. 272.

[8] F. Bečvář, J. Čížek, L. Lešták, I. Novotný, I. Procházka, F. Šebesta: Nucl. Instr. Meth. A Vol. 443 (2000), p. 557.

[9] J. Čížek, I. Procházka, B. Smola, I. Stulíková, R. Kužel, Z. Matěj, V. Cherkaska, phys. stat. sol. (a) Vol. 203 (2006), p. 466.

[10] H.E. Kissinger, Annal. Chem. Vol. 29 (1957), p. 1702.

[11] T. J. Pike, B. Noble, J. Less-Common Met. Vol. 30 (1973), p. 63.

[12] R. Ferragut, F. Moia, F. Fiori, D. Lussana, G. Riontino, J. Alloys Compd. Vol. 495 (2010), p. 408.

[13] M. Abdelrahman, P. Badawi: Jpn. J. Appl. Phys. Vol. 35 (1996), p. 4728.

[14] J. Čížek, I. Procházka, B. Smola, I. Stulíková, V. Očenášek, R.K. Islamgaliev, O. Kulyasova, Defect and Diffusion Forum Vols. 273-276 (2008), p. 75.

[15] J. Čížek, I. Procházka, B. Smola, I. Stulíková, M. Vlach, V. Očenášek, O.B. Kulyasova, R.K. Islamgaliev, Int. J. Mat. Res. Vol. 100 (2009), p. 780.

[16] J. Čížek, I. Procházka, B. Smola, I. Stulíková, V. Očenášek, J. Alloys Compd. Vol. 430 (2007), p. 92.

[17] J. Čížek, I. Procházka, B. Smola, I. Stulíková, V. Očenášek, R.K. Islamgaliev, O. Kulyasova, Mater. Sci. Forum Vol. 633-634 (2010), p. 353.

Recent Advances in Mass Transport in Materials
10.4028/www.scientific.net/DDF.322

Influence of Deformation on Precipitation Kinetics in Mg-Tb Alloy
10.4028/www.scientific.net/DDF.322.151

DOI References
[1] L.L. Rokhlin, Magnesium Alloys Containing Rare Earth Metals, Taylor and Francis, London (2003).
doi:10.4028/www.scientific.net/MSF.419-422.291

[3] B.L. Mordike: Mat. Sci. Eng. A Vol. 324 (2002), p.103.
doi:10.1016/S0921-5093(01)01290-4

[10] H.E. Kissinger, Annal. Chem. Vol. 29 (1957), p.1702.
doi:10.1021/ac60131a045

[11] T. J. Pike, B. Noble, J. Less-Common Met. Vol. 30 (1973), p.63.
doi:10.1016/0022-5088(73)90007-6

[12] R. Ferragut, F. Moia, F. Fiori, D. Lussana, G. Riontino, J. Alloys Compd. Vol. 495 (2010), p.408.
doi:10.1016/j.jallcom.2009.10.111